sulfuric acid as estimated from cyclic voltammetry at 200 mV s^{-1} is 5.2×10^{-2} F cm^{-2}. This compares favorably with the value of 1.2×10^{-2} F cm^{-2} for a film of ePt of similar thickness. The complex impedance of the double layer showed a capacitance of 5.1×10^{-2} F cm^{-2} and an effective series resistance of 0.8 ohm cm^2 at 1 Hz. The volumetric capacitance, estimated to be ~200 F cm^{-3}, is typical of the best candidate materials for electrochemical capacitors (*20*). The impedance was found to decrease with frequency according to $(i\omega)^{-0.9}$ up to the highest measurement frequency (6.5×10^3 Hz). This behavior is consistent with that observed for ePt. Any Warburg impedance due to the electrolyte resistance in the pores (*21*) was below the detection level, and therefore H_l-ePt can be expected to perform well as an electrochemical capacitor at high power and high frequency.

Our results show that electrodeposition of metals from appropriate salts dissolved in the aqueous domains of the lyotropic liquid crystalline phases of nonionic surfactants produces metal films that combine well-defined porous nanostructures, high specific surface areas, electrical connectivity, fast electrolyte diffusion, and good mechanical and electrochemical stability. In these films, the diameters of the holes are determined by the length of the alkyl chain of the surfactant used in the plating mixture, whereas the geometric disposition of the channels is determined by the architecture of the liquid crystalline phase. Because both of these parameters are under direct experimental control, electrodeposition from liquid crystalline plating mixtures provides a versatile route to creating mesoporous metal films that could represent new generations of electrode materials for use in batteries, fuel cells, sensors, and electrochemical capacitors.

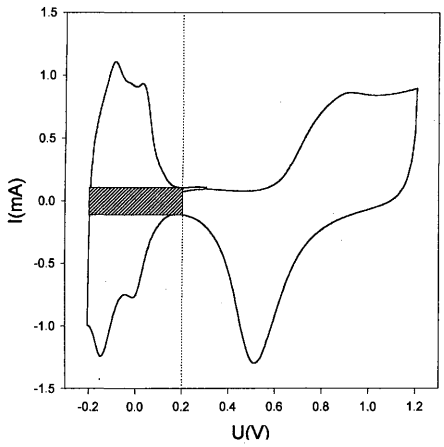

Fig. 3. Plot of current passed (I) while linearly scanning the applied voltage (U relative to the SCE) for H_l-ePt, recorded with a scan rate of 200 mV s^{-1} in 2 M aqueous sulfuric acid at 25°C. The platinum was electrodeposited at 65°C onto a 0.008-cm^2 polished gold electrode. The potential was stepped from +0.6 V versus the SCE to −0.1 V versus the SCE until a charge of −50 mC was passed. The surface area of the washed platinum deposit was determined from the charge associated with the hydrogen adsorption and desorption process (in the region +0.2 $V_{cathodic} \rightarrow$ −0.2 V → +0.2 V_{anodic}). The capacitive charge (shaded region) was not included. The surface area was determined to be 5.47 cm^2, which implies a roughness factor of ~680.

REFERENCES AND NOTES

1. P. Behrens, *Adv. Mater.* **5**, 127 (1993).
2. P. T. Tanev, M. Chibwe, T. J. Pinnavaia, *Nature* **368**, 321 (1994).
3. D. Antonelli and J. Ying, *Curr. Opin. Colloid Surf. Sci.* **1**, 523 (1996).
4. C. T. Kresge, M. E. Leonowicz, W. J. Roth, J. C. Vartuli, J. S. Beck, *Nature* **359**, 710 (1992).
5. C.-F. Cheng, Z. Luan, J. Klinowski, *Langmuir* **11**, 2815 (1995).
6. J. S. Beck *et al.*, *J. Am. Chem. Soc.* **114**, 10834 (1992).
7. A. Monnier *et al.*, *Science* **261**, 1299 (1993).
8. Q. Huo *et al.*, *Nature* **368**, 317 (1994).
9. S. A. Bagshaw, E. Prouzet, T. J. Pinnavaia, *Science* **269**, 1242 (1995).
10. G. S. Attard, J. C. Glyde, C. G. Göltner, *Nature* **378**, 366 (1995).
11. F. Leroux, B. E. Koene, L. F. Nazar, *J. Electrochem. Soc.* **143**, L181 (1996).
12. S. Ye, A. K. Vijh, L. H. Dao, *ibid.*, p. L7.
13. W. G. Pell and B. E. Conway, *J. Power Sources* **63**, 255 (1996).
14. J. Wang and L. Agnes, *Anal. Chem.* **64**, 456 (1992).
15. G. S. Attard, J. M. Corker, C. G. Göltner, S. Henke, R. H. Templer, *Angew. Chem. Intl. Ed. Engl.* **36**, 1315 (1997).
16. W. Torres and M. A. Fox, *Chem. Mater.* **4**, 583 (1992).
17. A. J. Bard, in *Electroanalytical Chemistry*, A. J. Bard, Ed. (Dekker, New York, 1976).
18. A. M. Feltham and M. Spiro, *Chem. Rev.* **71**, 187 (1971).
19. J. Bett, J. Lundquist, E. Washington, P. Stonehart, *Electrochim. Acta* **18**, 343 (1973).
20. S. Sarangapani, B. V. Tilak, C.-P. Chen, *J. Electrochem. Soc.* **143**, 3791 (1996).
21. R. De Levie, *Electrochim. Acta.* **9**, 1231 (1964).

22. This work is funded through a grant from the Engineering and Physical Sciences Research Council of the United Kingdom. The authors thank B. Cressey and Q. X. Tong of Molecular Imaging for assistance with the TEM and STM studies, respectively.

24 July 1997; accepted 22 September 1997

A Porous Silicon-Based Optical Interferometric Biosensor

Victor S.-Y. Lin, Kianoush Motesharei, Keiki-Pua S. Dancil, Michael J. Sailor,* M. Reza Ghadiri*

A biosensor has been developed based on induced wavelength shifts in the Fabry-Perot fringes in the visible-light reflection spectrum of appropriately derivatized thin films of porous silicon semiconductors. Binding of molecules induced changes in the refractive index of the porous silicon. The validity and sensitivity of the system are demonstrated for small organic molecules (biotin and digoxigenin), 16-nucleotide DNA oligomers, and proteins (streptavidin and antibodies) at pico- and femtomolar analyte concentrations. The sensor is also highly effective for detecting single and multilayered molecular assemblies.

Biosensors have been developed to detect a variety of biomolecular complexes, including oligonucleotides (*1–4*), antibody-antigen interactions (*5*, *6*), hormone-receptor interactions (*7*), enzyme-substrate interactions (*8*, *9*), and lectin-glycoprotein interactions (*10*). In general, biosensors consist of two components: a highly specific recognition element and a transducer that converts the molecular recognition event into a quantifiable signal. Signal transduction has been accomplished with electrochemical (*11*), field-effect transistor (*12*), optical absorption, fluorescence, interferometric (*13*) and other devices (*14*). Here we describe an optical interferometric transducer scheme based on inexpensive and readily available optically flat thin films of porous silicon (PSi). This material has been used for highly sensitive detection of small molecules (biotin and the steroid digoxigenin), short DNA oligonucleotides (16-nucleotide oligomers), and proteins (streptavidin and antibodies). Most notably, the sensor can be highly effective in detecting multiple layers of biomolecular interactions, termed "cascade sensing," including sensitive detection of small molecules.

Recent studies have shown that certain electrochemical etches of single-crystal *p*-type (boron-doped) Si wafers produce microporous material (PSi) that displays well-resolved Fabry-Perot fringes in its reflectometric interference spectrum (*15*). In our

V. S.-Y. Lin, K. Motesharei, M. R. Ghadiri, Departments of Chemistry and Molecular Biology, and The Skaggs Institute for Chemical Biology, The Scripps Research Institute, La Jolla, CA 92037, USA.
K.-P. S. Dancil and M. J. Sailor, Department of Chemistry and Biochemistry, University of California, San Diego, La Jolla, CA 92093–0358, USA.

*To whom correspondence should be addressed.

sensor (Fig. 1), reflection of white light at the top and bottom of the PSi layer results in an interference pattern that is related to the effective optical thickness (product of thickness L and refractive index n) of the film by Eq. 1 (*16*)

$$m\lambda = 2nL \quad (1)$$

where m is the spectral order and λ is the wavelength of light. Binding of an analyte to its corresponding recognition partner, immobilized on the PSi substrate, results in a change in the refractive index of the layer medium and is detected as a corresponding shift in the interference pattern. Electrochemical etching of Si generates a thin (1 to 5 μm) layer of porous Si on the Si substrate with cavities as wide as 200 nm in diameter, providing a large surface area for biomolecular interaction inside the porous layer. The films are uniform and sufficiently transparent to display Fabry-Perot fringes in their optical reflection spectrum (*17*).

We used DNA oligonucleotide–derivatized PSi films to test the selectivity and limits of detection (*18*). In the presence of complementary DNA (cDNA) sequences (DNA concentrations ranging from 2×10^{-15} to 2×10^{-6} M), pronounced wavelength shifts in the interference pattern of the PSi films were observed (Fig. 2, A and B). Under similar conditions but in the presence of non-cDNA sequences, no significant shift in the wavelength of the interference fringe pattern was detected—only minor amplitude fluctuations were observed. We used fluorescence spectroscopy to independently investigate the surface coverage of immobilized DNA on PSi and the rate of analyte diffusion into the matrix. Solutions of fluorescein-labeled cDNA oligonucleotides were placed in fluorescence cuvettes, and the DNA-derivatized PSi sample was then added to the cell without stirring. At the lowest DNA concentrations used, the fluorescence intensity of the samples decreased to an asymptotic limit in 40 min (similar equilibration times were observed in the interferometric measurements described above). The data indicate that 1.1×10^{-12} mol of DNA is covalently bound in the region beneath a 1-mm^2 spot on the PSi layer (calculated from standardized fluorescence titration curves). The data obtained from the reflectometric interference measurements also provided a similar coverage number. The lowest DNA concentration measured with the PSi interferometric sensor was 9 fg/mm^2 (Fig. 3). For comparison, the detection limits of current technologies are as follows: 1 pg/mm^2 for interferometry, 5 pg/mm^2 for grating couplers, and 0.3 pg/mm^2 for surface plasmon resonance (*19*).

We used biotinylated PSi to investigate sensing of multiple layers of biomolecular

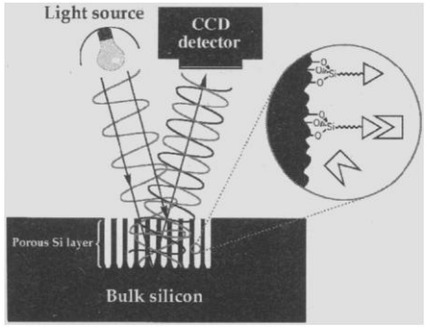

Fig. 1. Schematic of the PSi-based optical interferometric biosensor. The silicon oxide surface of the porous layer can be modified to express various molecular recognition elements (such as oligonucleotides, biotin, or antibodies). Reflection of white light (W-lamp source) at the top and bottom of the PSi layer results in an interference pattern (Fabry-Perot fringes). The reflectometric interference spectrum is sensitive to the refractive index of the PSi matrix. Interactions of the molecular species with their recognition partners immobilized on the surface induce a change in the refractive index of the nanocrystalline semiconductor, giving rise to wavelength shifts in the fringe pattern that can be easily detected [charge-coupled device (CCD) camera] and quantified.

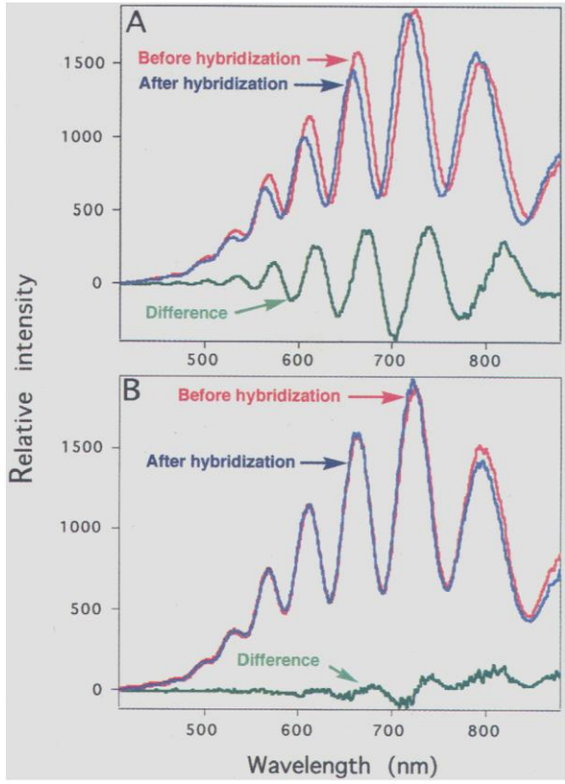

Fig. 2. Interferometric reflectance spectra of DNA-modified PSi layers. Experiments were measured for two DNA sequences (DNA-A: 5′-pGC CAG AAC CCA GTA GT-3′ and DNA-B: 5′-CCG GAC AGA AGC AGA A-3′) and corresponding complementary strands (DNA-A′ and DNA-B′). For clarity, only one set of data is shown in each case. (**A**) The Fabry-Perot fringes from a PSi surface derivatized with DNA-A ("before hybridization," red trace) shift to shorter wavelength upon exposure to a 2×10^{-12} M solution of DNA-A′ (the cDNA sequence to DNA-A) in 1 M NaCl(aq) ("after hybridization," blue trace). The net change in effective optical thickness (from 7986 to 7925 nm) upon DNA-A′ recognition is represented by the difference between the two interference spectra ("difference," green trace). (**B**) The control experiment, showing the Fabry-Perot fringes of a DNA-A–derivatized PSi surface before and after exposure to a 2×10^{-12} M solution of DNA-B (non-cDNA sequence) in 1 M NaCl(aq). No wavelength shift was observed up to the measured concentration of 10^{-9} M DNA-B.

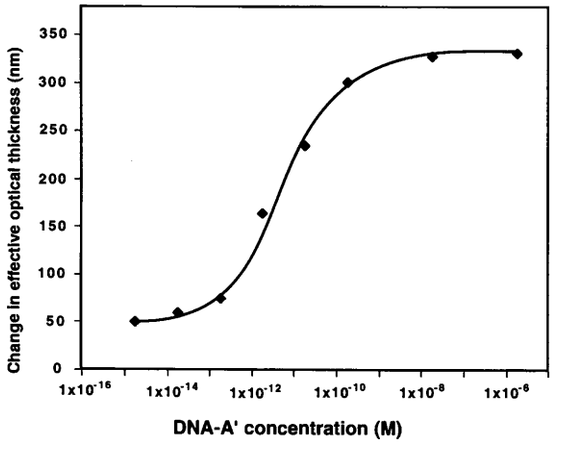

Fig. 3. Change in effective optical thickness in a DNA-A–modified PSi layer as a function of DNA-A′ (the cDNA sequence) concentration [25°C, 1 M NaCl(aq); equilibration time, 30 min]. The changes correspond to a net decrease in effective optical thickness upon hybridization by DNA-A′. The value of the change in effective optical thickness is defined as the measured effective optical thickness before hybridization minus the effective optical thickness 30 min after addition of the solution of DNA-A′. The sensor is responsive to femtomolar DNA concentrations.

interactions (cascade sensing) and small molecule detection (*20*). Exposure of a biotinylated PSi sample to a streptavidin-containing solution resulted in a large blue shift of the interference fringes that corresponded to a decrease in the measured effective optical thickness (the lowest streptavidin concentration used was 10^{-14} M) (Fig. 4A). Control experiments in which a biotinylated PSi sample was exposed to inactivated streptavidin (streptavidin presaturated with biotin) did not display perceptible shifts in the interference pattern. The biotin-streptavidin monolayer surface was treated with biotinylated antibody to mouse immunoglobulin G (IgG, from goat IgG). Binding of this secondary antibody to the surface was indicated by a further decrease in effective optical thickness of the monolayer (the lowest tested concentration used was 10^{-12} M) (Fig. 4B). Treatment of the secondary antibody sample with antibody to digoxigenin (mouse IgG) at a concentration of 10^{-8} M caused a further decrease in the effective optical thickness of the monolayer (Fig. 4C). Remarkably, the interaction of digoxigenin (10^{-6} M), a steroid with molecular weight (MW) of 392, with the IgG antibody to digoxigenin bound to the PSi surface was also detected (Fig. 4D).

To rule out the possibility of nonspecific interaction, we subjected a nonbiotinylated surface to the same experimental protocol as described above. No measurable change in the effective optical thickness was observed on treatment with streptavidin, secondary antibody, primary antibody, and digoxigenin. As in all affinity-based sensors, interference arising from nonspecific interactions with the recognition elements is to be expected. Interference from nonspecific adsorption to the surface-bound antibodies was not tested in the current study. We were also able to detect the relatively small biotin molecule (MW = 244) at concentrations as low as 10^{-12} M with biotin-streptavidin–modified PSi. The sensitivity of the system described is remarkable, especially in light of its ability to detect multiple layers of large- and small-molecule interactions even in cases where the recognition sites are apparently far removed (on the order of nanometers) from the Si surface.

Our hypothesis regarding this sensitivity is as follows. Selective incorporation or concentration of an organic analyte in the PSi layer can modify the refractive index in two ways: It should increase the average n of the medium in the pores by replacing water (n = 1.33) with organic matter (n = 1.45), and it can also decrease the n of PSi by modifying the carrier concentration in the semiconductor (*21–25*). A net increase in n is expected to shift the interference spectrum to longer wavelength, but in all of our binding studies, a shift to shorter wavelength was seen, an indication that the induced change in the semiconductor overwhelms the change in n occurring in the solution phase.

The reduction of n of the nanocrystalline Si substrate on binding of biomolecules is unexpected but is apparently responsible for the high sensitivity of this technique. The effect of interfacial capacitance on n is not easy to predict, especially for a material that is strongly absorbing in the wavelength region of observation (*26*). However, binding of molecules to semiconductor surfaces is known to modify carrier concentrations substantially (*22*, *23*). For example, exposure of PSi to alcohols or water vapor can dramatically increase the conductivity of the porous layer (*24*), and binding of molecules to II-VI semiconductor surfaces substantially modifies carrier concentration in the space-charge region (*27*). In our system, molecular complexation presumably reduces interfacial capacitance, as predicted by the Gouy-Chapman double-layer model (*28*), and in turn expels charge carriers from the PSi fibrils into the bulk semiconductor. Reduction of the carrier density effectively reduces the n of the layer, shifting the Fabry-Perot fringes to higher energy.

We observed a similar effect in test experiments with aqueous NaCl solutions and unmodified oxidized PSi samples; the Fabry-Perot fringes initially shifted to the blue as NaCl was added to a sample immersed in deionized water, and then at higher NaCl concentrations (after establishment of a large double-layer capacitance), an increase in ion concentration caused a red shift in the fringes. Whether or not a double-layer capacitance-induced dielectric change is the correct mechanism, the change in n of the PSi layer is much greater than the change expected by replacement of water with biomolecules and provides higher sensitivity over existing optical interferometric detection schemes.

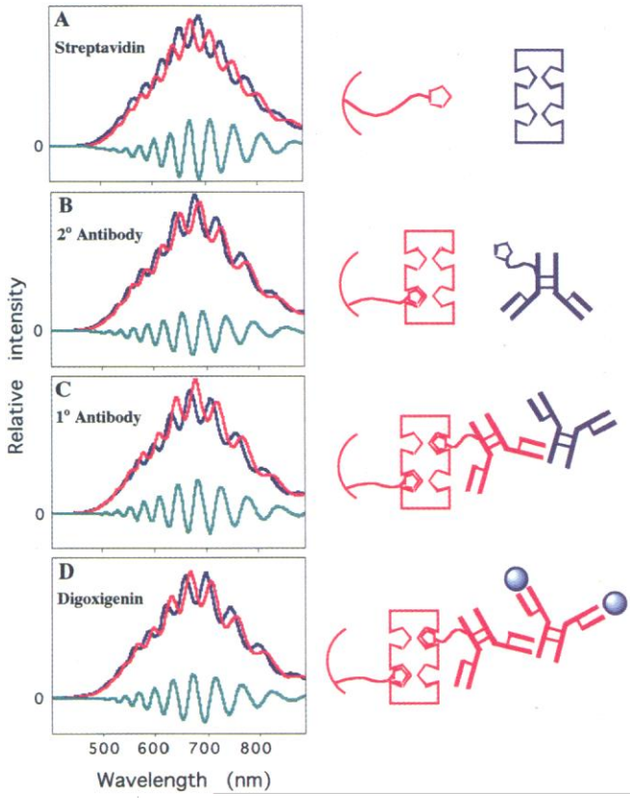

Fig. 4. Cascade sensing and reflectometric interference spectra of a multilayered molecular assembly. (**A**) A biotinylated PSi sample (red) treated with a 5×10^{-7} M streptavidin solution (blue) (effective optical thickness decreased from 12,507 to 11,994 nm). (**B**) Streptavidin-bound PSi sample (red) treated with a 10^{-8} M solution of biotinylated goat IgG antibody (2° antibody to mouse antibody to digoxigenin) (blue) (effective optical thickness decreased from 11,997 to 11,767 nm). (**C**) A biotinylated IgG antibody (to mouse antibody to digoxigenin) bound to a PSi sample (red) treated with a 10^{-8} M solution of mouse IgG antibody to digoxigenin (1° antibody) (blue) (effective optical thickness decreased from 11,706 to 11,525 nm). (**D**) A mouse IgG antibody to digoxigenin bound to a PSi sample (through the complex shown) (red) treated with 10^{-6} M digoxigenin solution (blue) (effective optical thickness decreased from 11,508 to 11,346 nm). The red traces correspond to the optical measurement made before exposure to the analyte of interest, the blue traces correspond to the measurement made after exposure, and the difference spectra (the difference between the red and blue traces) are represented as the green trace. All experiments were performed in 0.5 M aqueous NaCl at 25°C.

REFERENCES AND NOTES

1. M. Chee *et al.*, *Science* **274**, 610 (1996).
2. E. M. Southern *et al.*, *Nucleic Acids Res.* **22**, 1368 (1994).
3. J. A. Ferguson, T. C. Boles, C. P. Adams, D. R. Walt, *Nature Biotechnol.* **14**, 1681 (1996).
4. M. Schena, D. Shalon, R. W. Davis, P. O. Brown, *Science* **270**, 467 (1995).
5. S. M. Barnard and D. R. Walt, *ibid.* **251**, 927 (1991).
6. P. S. Stayton *et al.*, *Nature* **378**, 472 (1995).
7. F. J. Rowell, *Biochem. Soc. Trans.* **19**, 32 (1991).
8. A. Riklin, E. Katz, I. Willner, A. Stocker, A. F. Buckmann, *Nature* **376**, 672 (1995).

9. R. V. Parthasarathy and C. R. Martin, *ibid.* **369**, 298 (1994).
10. Y. Shinohara *et al.*, *J. Biochem.* **117**, 1076 (1995).
11. J. J. Hickman, D. Ofer, P. E. Laibinis, G. M. Whitesides, M. S. Wrighton, *Science* **252**, 688 (1991).
12. H. M. McConnell *et al.*, *ibid.* **257**, 1906 (1992).
13. A. Brecht and G. Gauglitz, *Biosens. Bioelectron.* **10**, 923 (1995).
14. W. Göpel *et al.*, Eds., *Sensors Update* (Wiley-VCH, Weinheim, Germany, 1989–1996), vols. 1–9.
15. V. V. Doan and M. J. Sailor, *Science* **256**, 1791 (1992).
16. B. Rossi, *Optics* (Addison-Wesley, Reading, MA, 1957).
17. Optically flat thin films of PSi were prepared by electrochemical etch of polished (100)-oriented *p*-type Si (B-doped, 3 ohm-cm resistivity) in a 1:1 98% ethanol:49% aqueous HF solution for 2 min at a current density of 50 mA/cm^2. Scanning electron microscopy and atomic force microscopy showed that PSi films prepared in this manner are 1 to 5 μm thick and contain pores with diameters up to 200 nm. The PSi matrix was modified by Br_2(g) oxidation in an evacuated chamber for 1 hour followed by hydrolysis in air.
18. For attachment of DNA, we synthesized a trimethoxy-3-bromoacetamidopropylsilane linker by reaction of bromoacetic acid with 1-(3-dimethylaminopropyl)-3-ethylcarbodiimide hydrochloride in CH_2Cl_2 solution. The linker product was purified by column chromatography on silica gel and characterized by ^{1}H nuclear magnetic resonance spectroscopy. The oxidized PSi samples were then exposed to a toluene solution of the linker for 2 hours. The sample was thoroughly rinsed with pure toluene and CH_2Cl_2 and dried overnight in vacuum. A purified (high-performance liquid chromatography) 5′-phosphorothiate oligonucleotide (DNA-A) (5′-pGC CAG AAC CCA GTA GT-3′) (236 μg, 47.7 nmol) was dissolved in a solution of (1:1:0.2 water/dimethyl-formamide/5% $NaHCO_3$(aq); pH 8.5) and the linker-derivatized PSi chip was immersed in the DNA solution for 2 hours. The presence of the DNA modification on the PSi surface (DNA-A) was confirmed by Fourier transfer infrared spectroscopy.
19. A. Brecht and G. Gauglitz, in *Frontiers in Biosensorics II: Practical Applications*, F. W. Scheller *et al.*, Eds. (Birkhäuser, Basel, Switzerland, 1997), pp. 1–16.
20. We prepared a linker with attached biotin by reaction of iodoacetyl-LC-biotin (Pierce Biochemicals) with 3-mercaptopropyltrimethoxysilane (Aldrich Chemicals) in dimethylformamide. After purification, the biotinylated linker was dissolved in ethanol or dimethylformamide, and the oxidized PSi sample was immersed in the solution for 12 hours. The sample was then rinsed thoroughly with ethanol and dried under a stream of N_2.
21. B. R. Hemenway, O. Solgard, D. M. Bloom, *Appl. Phys. Lett.* **55**, 349 (1989).
22. I. Schechter, M. Ben-Chorin, A. Kux, *Anal. Chem.* **67**, 3727 (1995).
23. D. Stievenard and D. Deresmes, *Appl. Phys. Lett.* **67**, 1570 (1995).
24. A. Motohashi *et al.*, *Jpn. J. Appl. Phys.* **35**, 4253 (1996).
25. K. Watanabe, T. Okada, I. Choe, Y. Sato, *Sens. Actuators B* **33**, 194 (1996).
26. C. Kittel, *Introduction to Solid State Physics* (Wiley, New York, ed. 6, 1986).
27. D. R. Neu, J. A. Olson, A. B. Ellis, *J. Phys. Chem.* **97**, 5713 (1993).
28. A. J. Bard and L. R. Faulkner, *Electrochemical Methods: Fundamentals and Applications* (Wiley, New York, 1980).
29. Financial support was provided by the Office of Naval Research (N000149511293) through the Multi-Disciplinary University Research Initiative of the Department of Defense. We thank J. E. Kyte and R. C. Dynes for helpful discussions. M.R.G. thanks the Scripps Research Institute for matching equipment funds. V.S.-Y.L. was supported under a Skaggs Institute postdoctoral fellowship, K.M. under an NIH postdoctoral fellowship (GM18309), and K.S.D. under an NIH predoctoral fellowship (2SO6 GM47165-06).

7 July 1997; accepted 23 September 1997

Quasi–Phase-Matched Third-Harmonic Generation in a Quasi-Periodic Optical Superlattice

Shi-ning Zhu,* Yong-yuan Zhu,* Nai-ben Ming*†

Quasi-periodic structure can be introduced into nonlinear optical materials such as $LiTaO_3$ crystals. Such structures were used for quasi–phase-matching second-harmonic generation. These materials are now shown to be able to couple second-harmonic generation and sum-frequency generation through quasi–phase-matching. The approach led to a direct third-harmonic generation with high efficiency through a coupled parametric process. The result verifies that high-order harmonics may be generated in a quadric nonlinear medium by a number of quasi–phase-matching processes, and therefore, exhibits a possible important application of quasi-periodic structure materials in nonlinear optics.

In dielectric crystals, the most important physical processes are the propagation and excitation of classical waves (optical and ultrasonic waves). The behavior of classical waves in a homogeneous dielectric crystal is the same as that in a continuous medium, because the wave vector of a classical wave is much smaller than the reciprocal vectors of crystal lattice. However, if some microstructure is introduced into a dielectric crystal, forming a superlattice, and if the reciprocal vectors of the superlattice are comparable with the classical wave vectors, the situation is quite different. The propagation of classical waves in a superlattice (classical system) is similar to the electron motion in a periodic potential of crystal lattice (quantum system). Thus, some ideas in solid-state electronics—for example, the reciprocal space, Brillouin zone, dispersion relation, and the like—may be used in classical wave processes. Such is the case for photonic band-gap materials (*1*). With classical systems, eigenvalues and eigenfunctions were measured directly (*2*). These are difficult if not impossible to obtain in quantum systems. On the other hand, the interactions between wave vectors of classical waves and reciprocal vectors of the superlattice may generate some new physical effects. In nonlinear optical fields, the interactions have led to new laser frequency generations in quasi–phase-matching (QPM) schemes from a number of optical superlattice crystals such as $LiNbO_3$, $LiTaO_3$, and $KTiOPO_4$ (*3*, *4*).

The above concepts may be equally applied to the quasiperiodic structure. Despite the large amount of research on the quasiperiodic structure since its discovery in 1984 (*5*), whether this kind of structure can be of any practical use remains undetermined. It was proposed that the quasi–phase-matching theory can be extended from periodic structures to quasiperiodic structures (*6*), which may find applications in nonlinear optics through the QPM method. With the development of the electric poling technique, ferroelectric crystals such as $LiTaO_3$, $LiNbO_3$, $KTiOPO_4$, and the like with quasiperiodically domain-inverted structure (hereafter we call it quasiperiodic optical superlattice, or QPOS) can be fabricated. We previously reported the experimental results of multiwavelength second-harmonic generation (SHG) in a Fibonacci QPOS $LiTaO_3$ (*6*). Because more reciprocal vectors can be provided by a QPOS, not only the quasi–phase-matched (QPM) multiwavelength SHG but also some coupled parametric processes, such as the third-harmonic generation (THG) and fourth-harmonic generation, can be realized with high efficiency. Taking THG as an example, we present our results using the second-order nonlinear optical processes in a QPOS $LiTaO_3$ crystal.

THG has a wide application as a means to extend coherent light sources to short wavelengths. The creation of the third harmonic directly from a third-order nonlinear process is of little practical importance because of the intrinsic low third-order optical nonlinearity. Conventionally, an efficient THG was achieved by a two-step process. Two nonlinear optical crystals are needed: the first one for SHG and the second one for sum-frequency generation (*7*). In this regard, QPOS has some advantages over the conventional method. Here, only one crystal is needed and the harmonic generation can be realized with high efficiency by using the largest nonlinear optical coefficient over the entire transparency range of the material.

A QPOS may be thought to contain two

National Laboratory of Solid State Microstructures, Nanjing University, Nanjing 210093, China, and Center for Advanced Studies in Science and Technology of Microstructures, Nanjing 210093, China.

*These authors contributed equally to this work.
†To whom correspondence should be addressed.